



**HAL**  
open science

## Collisional excitation of c-MgC<sub>2</sub> by Helium

M. M'Hamdi, C T Bop, F Lique, A. Ben Houria, K. Hammami

► **To cite this version:**

M. M'Hamdi, C T Bop, F Lique, A. Ben Houria, K. Hammami. Collisional excitation of c-MgC<sub>2</sub> by Helium. Monthly Notices of the Royal Astronomical Society, 2024, 536 (2), pp.1791-1798. 10.1093/mnras/stae2688 . hal-04877501v2

**HAL Id: hal-04877501**

**<https://hal.science/hal-04877501v2>**

Submitted on 9 Jan 2025

**HAL** is a multi-disciplinary open access archive for the deposit and dissemination of scientific research documents, whether they are published or not. The documents may come from teaching and research institutions in France or abroad, or from public or private research centers.

L'archive ouverte pluridisciplinaire **HAL**, est destinée au dépôt et à la diffusion de documents scientifiques de niveau recherche, publiés ou non, émanant des établissements d'enseignement et de recherche français ou étrangers, des laboratoires publics ou privés.



Distributed under a Creative Commons Attribution 4.0 International License

# Collisional excitation of c-MgC<sub>2</sub> by Helium

M. M'hamdi,<sup>1</sup>★ C. T. Bop,<sup>2</sup>★ F. Lique,<sup>2</sup>★ A. Ben Houria<sup>1</sup> and K. Hammami<sup>1</sup>

<sup>1</sup>LSAMA, Department of Physics, Faculty of Sciences, Tunis El-Manar University, 1060 Tunis, Tunisia

<sup>2</sup>Univ Rennes, CNRS, IPR (Institut de Physique de Rennes) – UMR 6251, F-35000 Rennes, France

Accepted 2024 December 2. Received 2024 November 28; in original form 2024 October 21

## ABSTRACT

The cyclic form of magnesium dicarbide molecule (c-MgC<sub>2</sub>) has been detected in the carbon-rich circumstellar envelope of IRC+10216 and is considered as a valuable tracer for characterizing the physical conditions of the surrounding gas. In order to make the most of c-MgC<sub>2</sub> observations and accurately derive the physical conditions of the media where c-MgC<sub>2</sub> is detected, radiative transfer modelling, including collisional and radiative (de-)excitations, have to be performed. Here, we study the excitation of c-MgC<sub>2</sub> induced by collisions with He (as a proxy for H<sub>2</sub>). A new 3D potential energy surface (PES) is constructed using highly correlated ab initio methods. This PES reveals a minimum with a well depth of 20.66 cm<sup>-1</sup> below the c-MgC<sub>2</sub>-He dissociation limit. Using this PES, we compute excitation cross sections for transitions between the low-lying rotational energy levels of c-MgC<sub>2</sub> using the time-independent quantum mechanical close-coupling formalism. These cross sections are then thermally averaged over a Boltzmann energy distribution in order to derive excitation rate coefficients at low temperatures ( $T \leq 30$  K). To evaluate the impact of these new rate coefficients on the interpretation of c-MgC<sub>2</sub> observational spectra, we perform radiative transfer calculations. We find that a very high gas density ( $n > 10^6$  cm<sup>-3</sup>) is needed in order for the collisional excitation to compete with the radiative de-excitation. We also find that the excitation temperatures of the observed lines predicted by our model differ by a factor two from the value derived from the observations in IRC+10216 circumstellar envelope, indicating that the excitation of c-MgC<sub>2</sub> may also be driven by a strong radiative pumping in such media. Therefore, a more sophisticated non-LTE modelling, that takes into account the collisional and radiative excitations as well as the radiative pumping, is required to accurately interpret the observational spectra of c-MgC<sub>2</sub>.

**Key words:** molecular data – molecular processes – radiative transfer – scattering – ISM: abundances – ISM: molecules.

## 1 INTRODUCTION

The IRC+10216 circumstellar envelope (CSE) is notably abundant in carbon-chain molecules, as well as in neutral and ionized metal-bearing species (Agúndez et al. 2012; Tuo et al. 2024). These latter species evolve principally within the outer layers of the IRC+10216 CSE and are subject to a complex gas phase chemistry (Mauron & Huggins 2010). Hence, the detection of various polyatomic metal-containing molecules, specifically MC<sub>n</sub>N and MC<sub>n</sub>H (where M represents a metallic element), has been possible in the IRC+10216 CSE (Cernicharo et al. 2019; Pardo et al. 2022; Cabezas et al. 2023). However, metal-bearing carbon-chain molecules (MC<sub>n</sub>) have remained elusive in this source, despite the substantial abundance of metal atoms.

Metal dicarbides (MC<sub>2</sub>) have long been anticipated to represent a significant portion of the gas toward evolved carbon stars, such as IRC+10216 since these compounds are likely to be formed through non-equilibrium gas-phase processes in cool, rarefied circumstellar envelopes and under thermochemical equilibrium conditions near

hot, dense stellar photospheres (Tsuji 1973; Turner 1991; Petrie 1996).

Among metal dicarbides, magnesium dicarbide (MgC<sub>2</sub>) – a highly polar molecule containing magnesium, one of the most abundant metallic element in space – stand out as particularly promising for astronomical detection. Then, thanks to high-resolution laboratory experiments (Changala et al. 2022), c-MgC<sub>2</sub> was recently identified as the carrier of numerous previously unassigned emission lines detected in surveys of the IRC+10216 CSE (Cernicharo, Guélin & Pardo 2004; Cernicharo et al. 2019; Pardo et al. 2022).

Changala et al. (2022) reported a c-MgC<sub>2</sub> column density of 10<sup>12</sup> cm<sup>-2</sup> derived from the analysis of a rotational diagram using a two-temperatures model. A two-temperatures model was used since the relative population of energy levels radiatively connected were supposed to be highly subthermal because of the strong dipole moment of the molecule ( $\mu = 7.9$  D; Itono et al. 2000) whereas the relative population of energy levels belonging to different  $k$ -ladder<sup>1</sup> were supposed to be thermalized (since they are not radiatively connected but only collisionally connected).

\* E-mail: [maroua.mhamdi@fst.utm.tn](mailto:maroua.mhamdi@fst.utm.tn) (MM); [cheikhdiiane.bop@ucad.edu.sn](mailto:cheikhdiiane.bop@ucad.edu.sn) (CTB); [françois.lique@univ-rennes.fr](mailto:françois.lique@univ-rennes.fr) (FL)

<sup>1</sup>The rotational energy levels of c-MgC<sub>2</sub> are labelled  $j_{k_a k_c}$ , with  $j$  being the total angular momentum and  $k_a$  and  $k_c$  its projections along the  $a$ - and  $c$ -axes of inertia. A  $k$ -ladder is the ensemble of rotational levels with the same  $k_a$ .

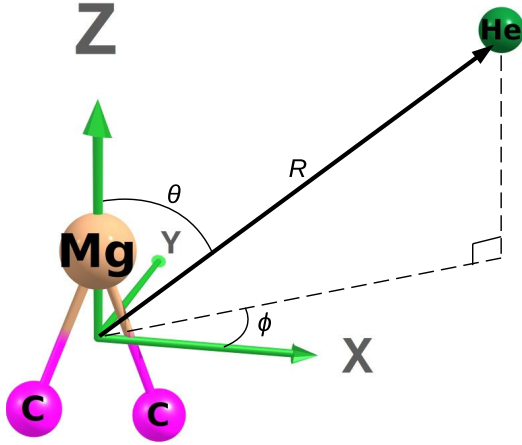


**Figure 1.** Jacobi coordinates system for the  $c\text{-MgC}_2\text{-He}$  complex.

Deriving the most accurate abundance of  $c\text{-MgC}_2$  in the IRC+10216 CSE can provide key insights for the understanding of dust formation and of ion–molecule reactions involving metal-bearing species (Changala et al. 2022). It is then crucial to check the validity of the use of a two-temperatures model and of a rotational diagram for deriving  $c\text{-MgC}_2$  abundance in the IRC+10216 CSE. The accurate determination of the  $c\text{-MgC}_2$  excitation conditions using radiative transfer models requires solving simultaneously the radiative transfer and the statistical equilibrium equations. Hence, accurate determination of the  $c\text{-MgC}_2$  abundance requires the prior calculation of excitation rate coefficients induced by collisions with the most abundant species since the collisional processes contribute, in competition with the radiative processes, to the (de-)excitation of molecular levels.

To the best of our knowledge, the scattering of  $c\text{-MgC}_2$  by any relevant astronomical projectile (He, H,  $\text{H}_2$ , and  $e^-$ ) has not been investigated. In this work, we investigate the excitation of  $c\text{-MgC}_2$  induced by collisions with He atoms (as a model for  $\text{H}_2$ , the dominant projectile in the IRC+10216 CSE). He is usually considered as a reasonable proxy for *para*- $\text{H}_2$  in its ground rotational state since both species have two electrons and a spherical structure. We compute the first interaction potential for the  $c\text{-MgC}_2\text{-He}$  complex and derive state-to-state excitation cross sections for rotational transitions induced by He collisions. The computational details are provided in Section 2, and the results are presented and discussed in Section 3. Section 4 explores the possible impact of the new rate coefficients on the excitation of  $c\text{-}^{24}\text{MgC}_2$  (hereafter  $c\text{-MgC}_2$ ) in the IRC+10216 carbon-rich CSE. Concluding remarks are presented in Section 5.

## 2 COMPUTATIONAL DETAILS

### 2.1 Potential energy surface

The potential energy surface (PES) calculation is conducted considering  $c\text{-MgC}_2$  as a rigid molecule with the equilibrium geometry of  $c\text{-MgC}_2$  estimated from the rotational constants reported by Changala et al. (2022). The  $c\text{-MgC}_2$  structure exhibits a triangular configuration. The C–C and the ionic  $\text{Mg}^+\text{-C}_2^-$  bond lengths are  $r_{\text{CC}} = 1.2706 \text{ \AA}$  and  $r_{\text{Mg-C}_2} = 1.9066 \text{ \AA}$ , respectively. Three coordinates are needed to calculate the  $c\text{-MgC}_2\text{-He}$  PES in the rigid-rotor approximation. We used the Jacobi coordinates system, as shown in Fig. 1 to describe the geometry of the  $c\text{-MgC}_2\text{-He}$  complex. The origin of the body-fixed coordinates system is placed at the

centre of mass of  $c\text{-MgC}_2$ . The  $C_2$  axis of the molecule aligns with the  $z$ -axis and  $c\text{-MgC}_2$  lies in the  $XZ$  plane so that the Mg atom points in the positive direction of the  $Z$ -axis. The distance between the origin of the coordinate system and the position of He atom is denoted  $R$ , whereas the body-fixed angles  $\theta$  and  $\phi$  describe the relative orientation. For the calculation of the PES, these angles are varied by a uniform step of  $10^\circ$  as  $0^\circ \leq \theta \leq 180^\circ$  and  $0^\circ \leq \phi \leq 90^\circ$ . The radial distance ranged from  $R = 4$  bohr to  $R = 20$  bohr with a progressively increasing step size, initially set at 0.25 bohr up to  $R = 10$  bohr, then 0.5 bohr up to  $R = 15$  bohr, and finally 1 bohr for larger distances. The interaction potential as a function of the Jacobi coordinates, i.e.  $V(R, \theta, \phi)$ , is calculated using the explicitly correlated coupled-clusters ab initio approach with single, double, and perturbative triple excitation [CCSD(T)-F12] (Knizia, Adler & Werner 2009) in conjunction with the augmented-correlation consistent-polarized valence triple zeta (aug-cc-pVTZ) basis sets (Kendall, Dunning & Harrison 1992). To address the size consistency problem of the CCSD(T)-F12 method, we subtract from the 3D-PES the residual of the interaction potential calculated for each orientation at  $R = 100$  bohr. In addition, we use the counterpoise procedure of Boys & Bernardi (1970):

$$V(R, \theta, \phi) = E_{\text{MgC}_2\text{-He}}(R, \theta, \phi) - E_{\text{MgC}_2}(R, \theta, \phi) - E_{\text{He}}(R, \theta, \phi), \quad (1)$$

where  $E_{\text{MgC}_2\text{-He}}$  is the electronic energy of the  $c\text{-MgC}_2\text{-He}$  complex, and the last two terms are the energies of the two fragments, all calculated using the full basis set of the entire system. All calculations were carried out using the MOLPRO quantum chemistry package code (Werner et al. 2015, a package of ab initio programs).

The comparison of radial potential energy cuts obtained using the present methodology and the gold standard CCSD(T) approach (Hampel, Peterson & Werner 1992) together with an extrapolation to the complete basis sets (CBS) limit (Feller 1992) is presented in Fig. 2. As one can see, the potential energy cuts obtained with the two approaches are in good agreement. Minor deviations (less than  $1 \text{ cm}^{-1}$ ) are found for the position of the minima that are not likely to strongly influence the scattering calculations. Hence, according to the test results presented in Fig. 2, the choice of the CCSD(T)-F12a method in conjunction with the aug-cc-pVTZ basis set is justified by a good convergence with the CCSD(T)/CBS, which is the reference in our case. In addition, the selected method allows for a much lower consumption of computer resources in comparison with CCSD(T)/CBS one.

### 2.2 Analytical fit

In order to use the computed PES in the scattering calculations, we derive an analytic representation of it. It is convenient to expand the PES, using spherical harmonics, as follows:

$$V(R, \theta, \phi) = \sum_{l,m} V_{lm}(R) \times \left( \frac{Y_l^m(\theta, \phi) + (-1)^m Y_l^{-m}(\theta, \phi)}{1 + \delta_{m,0}} \right), \quad (2)$$

where  $Y_l^m(\theta, \phi)$  are normalized spherical harmonics,  $\delta_{m,0}$  is the Kronecker symbol, and  $V_{lm}(R)$  are the radial functions required to compute the matrix elements of the potential during the scattering calculations.

By definition,  $l$  represents a non-negative integer ranging from zero to  $l_{\text{max}}$ , while  $m$  is constrained between zero and  $l$ . Due to the  $C_{2v}$  symmetry of  $c\text{-MgC}_2$ , only even integers are allowed for  $m$ . In our analytical expansion, we fix  $l_{\text{max}} = 12$ , and  $m$  is varied up to the minimum of  $\{l, 6\}$ , resulting in a total of 40 radial expansion

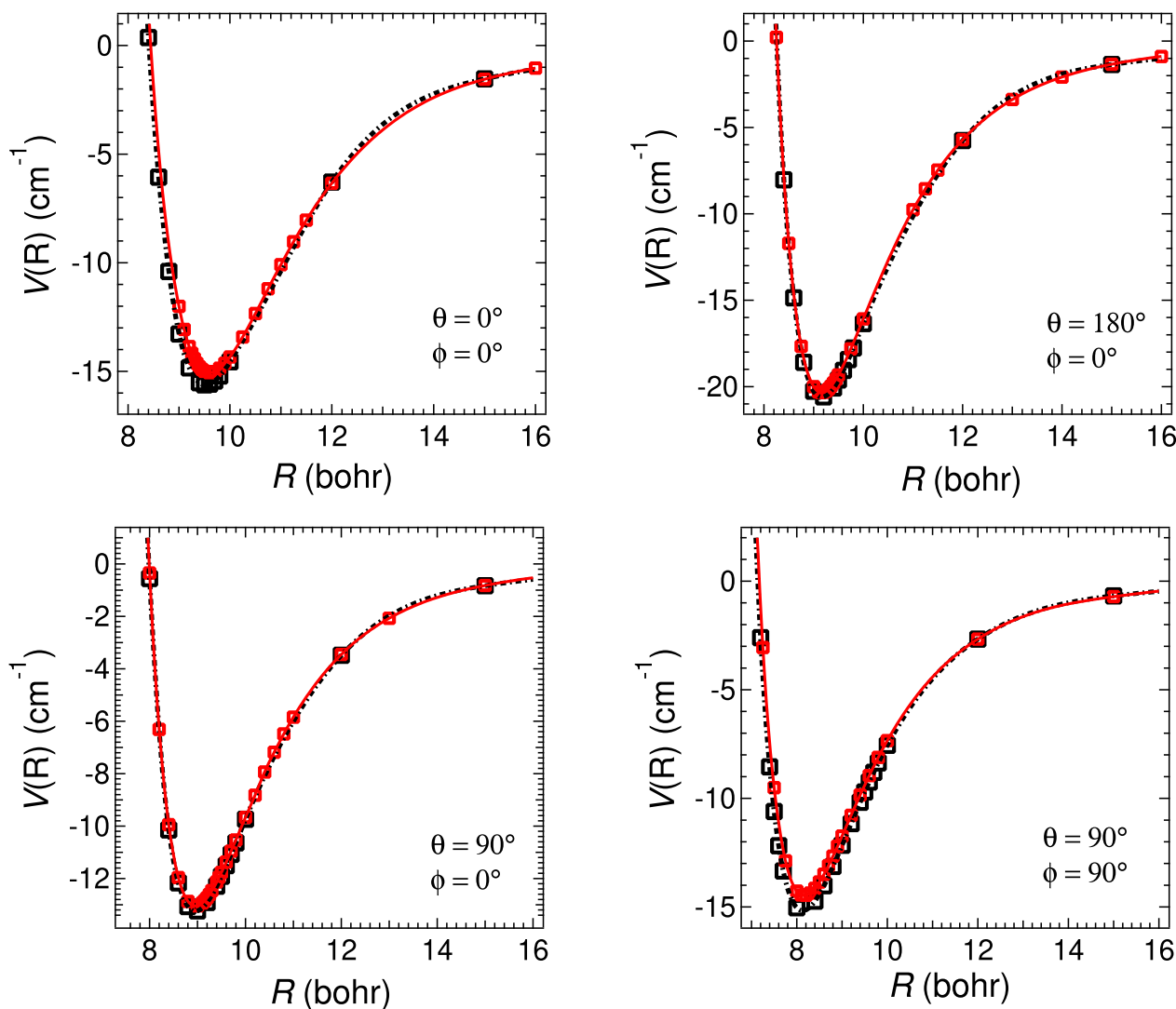


**Figure 2.** *c*-MgC<sub>2</sub>-He PES cuts obtained using the CCSD(T)-F12/AVTZ (solid line) and CCSD(T)/CBS (dashed line) methods.

coefficients. These  $R$ -dependent terms are refined using cubic spline interpolation routine for  $4 \text{ bohr} \leq R \leq 20 \text{ bohr}$  and extrapolated in the short and long ranges by the VSTAR routine of MOLSCAT (Hutson & Green 1994) as follows:

$$\begin{aligned} V_{lm}(R) &= a_{lm} \times \exp(-b_{lm}R), \text{ if } R < 4.0 \text{ bohr} \\ V_{lm}(R) &= c_{lm} \times R^{-d_{lm}}, \text{ if } R > 20.0 \text{ bohr} \end{aligned} \quad (3)$$

where  $a_{lm}$ ,  $b_{lm}$ ,  $c_{lm}$ , and  $d_{lm}$  are constant automatically calculated by MOLSCAT from the  $V_{lm}(R)$  radial functions.

## 2.3 Scattering calculations

### 2.3.1 Rotational energy levels of *c*-MgC<sub>2</sub>

Within a large dipole moment of 7.9 D lying along the  $a$ -axis of rotation that has the smallest moment of inertia, *c*-MgC<sub>2</sub> is an  $a$ -type asymmetric top molecule (Itono et al. 2000). The rotational energy levels of *c*-MgC<sub>2</sub> depend upon three quantum numbers: the total angular momentum ( $j$ ) and its projections  $k_a$  and  $k_c$  along the  $a$ - and  $c$ -axes, corresponding to those with the smallest and largest moments of inertia, respectively. Because of the  $C_{2v}$  symmetry, one could expect two nuclear spin configurations for *c*-MgC<sub>2</sub> but only

**Table 1.** Rotational and centrifugal distortion constants for *c*-MgC<sub>2</sub>. All constants are in  $\text{cm}^{-1}$ .

$A = 0.384$	$D_J = 4.821 \times 10^{-7}$
$B = 0.313$	$D_{JK} = 81.764 \times 10^{-7}$
$C = 1.731$	$D_K = -12.622 \times 10^{-7}$

one exists because of the spin statistics for the identical carbon nuclei. Hence, while  $k_c$  may take either even or odd values,  $k_a$  must be even. In practice,  $k_a$  ranges from zero to  $j$  and  $k_c$  is equal to  $j$  (when  $k_a$  is zero), and takes values from  $\{j - k_a, j - k_a + 1\}$  (when  $k_a$  is non-zero).

The rotational ( $A$ ,  $B$ , and  $C$ ) and centrifugal distortion ( $D_J$ ,  $D_{JK}$ , and  $D_K$ ) constants used in this work are derived from a least-squares fit using both astronomical and laboratory emission lines of *c*-MgC<sub>2</sub> (Changala et al. 2022) (see Table 1).

### 2.3.2 State-to-state cross sections

The analytical PES is incorporated into the MOLSCAT scattering code (Hutson & Green 1994) to compute state-to-state rotational cross

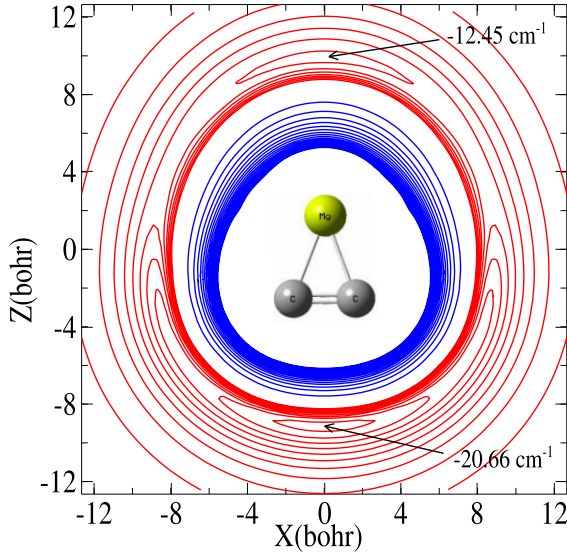


**Figure 3.** Contour plot of the c-MgC<sub>2</sub>–He interaction potential as a function of the  $x$  and  $z$  coordinates, where  $x = R \sin \theta \cos \phi$  and  $z = R \cos \theta$ .

sections ( $\sigma_{j_{k_a, k_c} \rightarrow j'_{k'_a, k'_c}}$ ) of c-MgC<sub>2</sub> induced by collisions with He as a function of the collision energy ( $E_k$ ). The scattering calculations were performed using the quantum mechanical close-coupling method (Arthurs & Dalgarno 1960) along with the hybrid (log derivative-airy) integrator of Alexander & Manolopoulos (1987).

In order to compute excitation cross sections for transitions involving rotational levels with internal energies lower than 44 cm<sup>-1</sup> ( $\simeq 65$  K), we include in the rotational basis all energy levels up to  $j_{k_a, k_c} = 16_{8,8}$ , which guarantee convergence of cross sections to better than 1 per cent. The integration length is automatically adjusted for the calculation of each partial cross section and the integration step is set low enough for all energy. The number of partial cross sections required to meet the convergence criteria was determined by setting a threshold of 0.005 Å<sup>2</sup> for the inelastic cross sections. The reduced mass of the c-MgC<sub>2</sub>–He complex is  $\mu = 3.696$  amu.

To accurately characterize the resonances appearing in the low energy excitation cross sections, we spanned the total energy  $E_{tot}$  range from 0.7 cm<sup>-1</sup> to 300 cm<sup>-1</sup> using a progressively increasing step size from 0.1 to 5 cm<sup>-1</sup>.

### 2.3.3 Collision rate coefficients

The excitation cross sections allows to derive collision rate coefficients ( $k_{j_{k_a, k_c} \rightarrow j'_{k'_a, k'_c}}^{c\text{-MgC}_2\text{-He}}$ ) for kinetic temperatures ( $T_k$ ) up to 30 K. In practice, we used the Maxwell–Boltzmann kinetic energy distribution to retrieve  $k$ , as follows:

$$k_{j_{k_a, k_c} \rightarrow j'_{k'_a, k'_c}}^{c\text{-MgC}_2\text{-He}}(T_k) = \left( \frac{8}{\pi \mu \beta} \right)^{1/2} \beta^2 \times \int_0^{+\infty} e^{-E_k \beta} E_k \sigma_{\alpha \rightarrow \alpha'}(E_k) dE_k, \quad (4)$$

where  $k_B$  is the Boltzmann constant and  $\beta = (k_B T_k)^{-1}$ .

## 3 RESULTS AND DISCUSSIONS

Fig. 3 presents a contour plot of the c-MgC<sub>2</sub>–He interaction potential for  $\phi = 0^\circ$  (i.e. He being in the plane of c-MgC<sub>2</sub>). As one can see, two distinct minima exist for  $\theta = 0^\circ$  and  $\theta = 180^\circ$ . The global minimum,

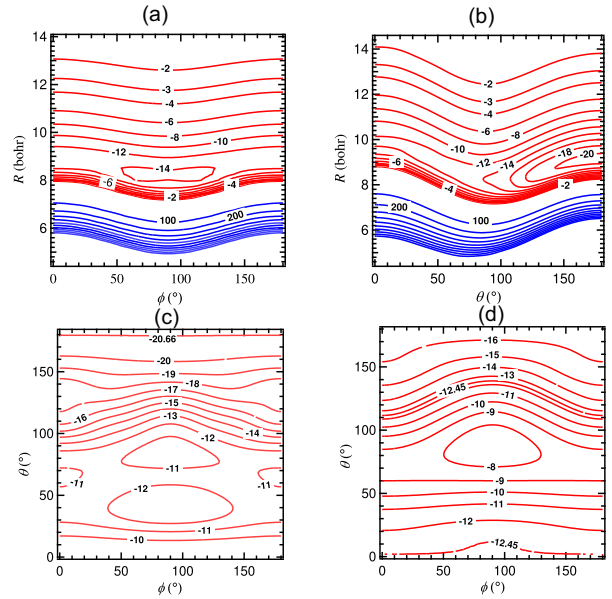


**Figure 4.** 2D cuts of the c-MgC<sub>2</sub>–He interaction potential, as a function of  $R$ ,  $\theta$ , and  $\phi$ . Panel (a) corresponds to  $\theta = 90^\circ$ , Panel (b) corresponds to  $\phi = 90^\circ$ , panel (c) to  $R = 9.25$  bohr while panel (d) corresponds to  $R = 10$  bohr. The energy zero is defined at infinite  $R$ .

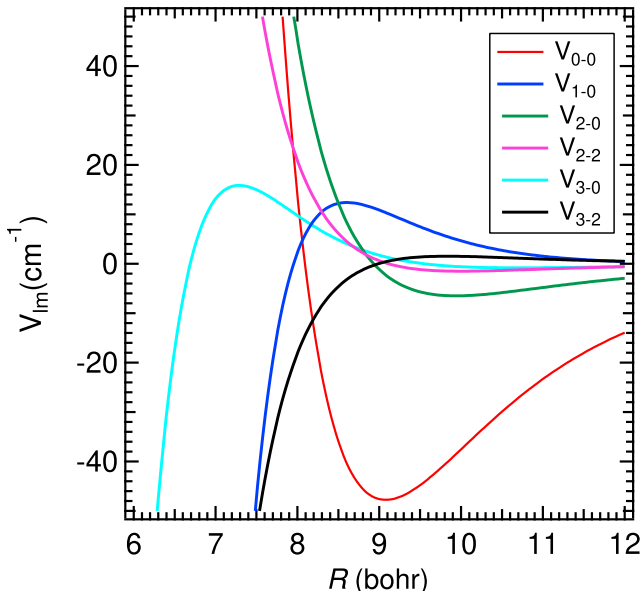
located at  $R = 9.25$  bohr,  $\theta = 180^\circ$ , and  $\phi = 0^\circ$ , corresponds to an interaction energy of  $-20.66$  cm<sup>-1</sup>. A shallower minimum occurs when the helium atom approaches to the magnesium atom, i.e.  $R = 10$  bohr,  $\theta = 0^\circ$ , and  $\phi = 0^\circ$ , with an interaction energy of  $-12.45$  cm<sup>-1</sup>.

Fig. 4 shows four cuts of the PES. Panel (a) and panel (b) illustrate the dependence of the potential on  $R$  and  $\phi$  at  $\theta = 90^\circ$  and on  $R$  and  $\theta$  at  $\phi = 90^\circ$ , respectively. Panels (c) and (d) depict the potential variation with  $\phi$  and  $\theta$  at fixed distances of  $R = 9.25$  and 10 bohr, respectively (the  $R$ -distances of the two minima). The global minimum of 20.66 cm<sup>-1</sup> can be seen in the panel (b) of Fig. 4.

Panels (c) and (d) of Fig. 4 shows again the existence of a global minimum at  $\theta = 180^\circ$  for  $R = 9.25$  bohr with a well depth of 20.66 cm<sup>-1</sup> and of the local minimum at  $\theta = 0^\circ$  for  $R = 10$  bohr. Overall, the interaction potential between c-MgC<sub>2</sub> and He exhibits significant anisotropy, as demonstrated by the distinct minima and the variations in potential energy across different orientations. Whereas the anisotropy of the PES with respect to  $\theta$  is large, the anisotropy of the PES with respect to  $\phi$  is however much weaker whatever the distance between the two colliders is. This also explains why only values of  $m \leq 6$  have been required for an accurate fit of the PES.

The first six radial terms of the analytical PES,  $V_{lm}(R)$  (see equation 2), are shown in Fig. 5. The isotropic ( $V_{00}$ ) radial term has a higher magnitude than all the anisotropic one ( $V_{l>0, m>0}$ ) for all  $R$ -distances. Then,  $V_{10}$  and  $V_{20}$  dominate the other terms. However,  $V_{10}$  and  $V_{20}$  have similar magnitudes, so that we anticipate that no clear propensity rules with respect to  $\Delta j = 1$  or  $\Delta j = 2$  transitions would be easily extracted from the excitation cross sections and rate coefficients analysis.

Fig. 6 shows the typical kinetic energy dependence of the de-excitation cross sections ( $\sigma_{j_{k_a, k_c} \rightarrow j'_{k'_a, k'_c}}$ ) of c-MgC<sub>2</sub> induced by collisions with He. Only transitions between energy levels with  $k_a = k'_a = 0$  are presented but transitions between levels with other  $k_a$  exhibit the same shape. At low collision energies ( $E_k \leq 20$  cm<sup>-1</sup>), several resonances are observed. These are a consequence of the two attractive potential wells (see above). Quasi-bound states may



**Figure 5.** The dependence on  $R$  of the first  $V_{lm}$  components.

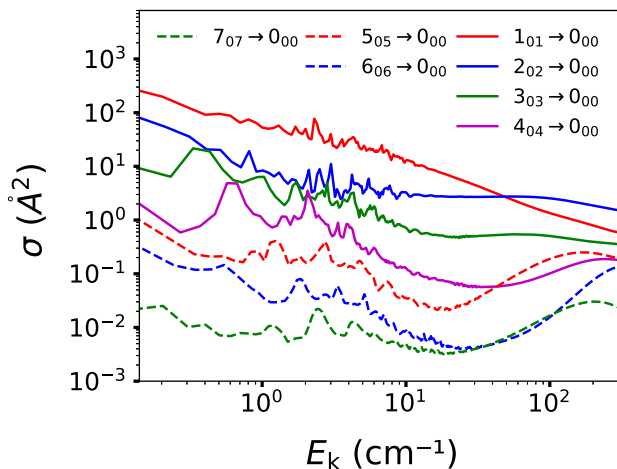


**Figure 6.** Kinetic energy dependence of the rotational cross sections of  $c\text{-MgC}_2$  in collision with He for de-excitation transition within the  $k_a = 0$  ladder.

arise from tunnelling through the centrifugal energy barrier (shape resonances) or from excitation of the  $c\text{-MgC}_2\text{-He}$  complex to a bend-stretch level which is energetically accessible because of the attractive wells but is asymptotically closed (Feshbach resonances).

One can also see that, at low kinetic energy ( $E_k \leq 30 \text{ cm}^{-1}$ ), the magnitude of the cross sections decreases with increasing  $\Delta j$ , showing a rotational energy gap-law dependence. At higher collisional energy, no clear propensity rules could be extracted.

Fig. 7 displays the kinetic temperature variation of the corresponding  $c\text{-MgC}_2\text{-He}$  collisional rate coefficients. One can note that the dominant rate coefficients exhibit a magnitude of the order of  $k \simeq 10^{-11} \text{ cm}^3 \text{ s}^{-1}$ , which is the typical value for rate coefficients involving collisions between He and a neutral target. Taken into account the high magnitude of  $c\text{-MgC}_2$  dipole moment, we anticipate that very high gas density would be required for collisional (de-)excitation to compete with radiative (de-)excitation.

$c\text{-MgC}_2\text{-He}$  rate coefficients for transitions with  $\Delta k_a = 0, 2, 4$ ;  $\Delta j = \Delta k_c = 0, 1, 2$  are presented in Fig. 8. This figure shows that the

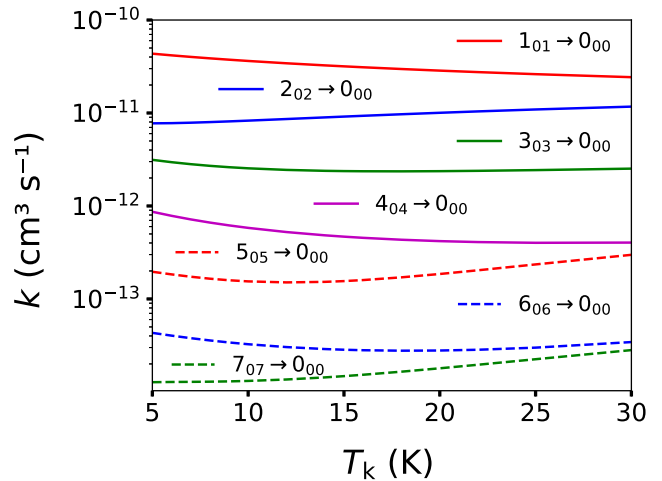


**Figure 7.** Kinetic temperature dependence of the rotational excitation rate coefficients of  $c\text{-MgC}_2$  induced by collisions with He for de-excitation transitions within the  $k_a = 0$  ladder.

rates for transitions with  $\Delta j = 0, 1$ ,  $\Delta k_a = 0$ , and  $\Delta k_c = 1$  are the largest. Such propensity rules in favour of  $\Delta k_a = 0$  and  $\Delta k_c = 0, \pm 1$  are typical for such molecules and have been already observed for  $\text{H}_2\text{O}$  (Faure et al. 2007) and  $\text{NH}_2$  (Bouhafaf et al. 2017).

#### 4 ASTROPHYSICAL MODELLING

In order to assess the impact of the new rate coefficients on the determination of the abundance of  $c\text{-MgC}_2$  in circumstellar media, we perform radiative transfer calculations under the escape probability formalism using RADEX (Van der Tak et al. 2007). The basic input is composed of  $c\text{-MgC}_2$  spectroscopic data (line frequencies, rotational energy levels, and Einstein coefficients) obtained from the Cologne Database for Molecular Spectroscopy (CDMS) portal (Endres et al. 2016) and of excitation rate coefficients induced by collisions with  $\text{H}_2$  ( $k_{j k_a, k_c \rightarrow j' k'_a, k'_c}^{c\text{-MgC}_2\text{-H}_2}(T_k)$ ). The latter data are derived from

the rate coefficients due to He-impact ( $k_{j k_a, k_c \rightarrow j' k'_a, k'_c}^{c\text{-MgC}_2\text{-He}(T_k)$ ) computed in this work by applying a mass scaling factor, as follows:

$$k_{j k_a, k_c \rightarrow j' k'_a, k'_c}^{c\text{-MgC}_2\text{-H}_2}(T_k) = \sqrt{\frac{\mu_{\text{MgC}_2\text{-He}}}{\mu_{\text{MgC}_2\text{-H}_2}}} \times k_{j k_a, k_c \rightarrow j' k'_a, k'_c}^{c\text{-MgC}_2\text{-He}(T_k), \quad (5)$$

where  $\sqrt{\frac{\mu_{\text{MgC}_2\text{-He}}}{\mu_{\text{MgC}_2\text{-H}_2}}} = 1.3823$  is the ratio of the reduced mass of the  $c\text{-MgC}_2\text{-He}$  and  $c\text{-MgC}_2\text{-H}_2$  systems.

The accuracy of such approximation is difficult to estimate. On the one hand, this approximation has been shown to be reasonable for heavy targets such as  $\text{HC}_3\text{N}$  (Wernli et al. 2007), AICN (Urzuá-Leiva & Denis-Alpizar 2020), or SiS (Lique et al. 2008). On the other hand, the large dipole moment of  $c\text{-MgC}_2$  may make its interaction with  $\text{H}_2$  probably quite different from that with He, leading to different magnitude for the corresponding He- and  $\text{H}_2$ -rate coefficients. Nevertheless, we checked that the excitation of  $c\text{-MgC}_2$  in the IRC+10216 CSE would not drastically change if the actual  $c\text{-MgC}_2\text{-H}_2$  rate coefficients are significantly larger (up to a factor of 3) than the present one estimated from He-rate coefficients.

The radiative transfer calculations are performed for  $T_k = [20 - 30] \text{ K}$ , varying the density of molecular hydrogen ( $n_{\text{H}_2}$ ) from  $10^2$  to  $10^{10} \text{ cm}^{-3}$ , setting the  $c\text{-MgC}_2$  column density at  $N = 10^{12} \text{ cm}^{-2}$ , employing a line width of  $14.5 \text{ km s}^{-1}$ . These parameters are compatible with the observations of Changala et al. (2022). We

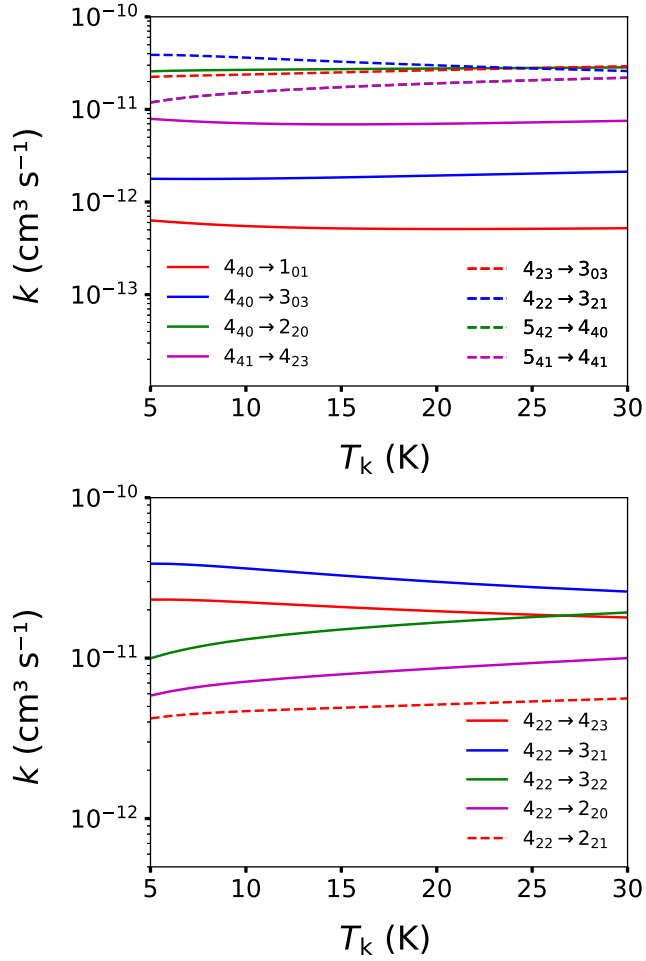


**Figure 8.** Kinetic temperature dependence of the rotational cross sections of  $c\text{-MgC}_2$  for transition between different  $k$ -ladder.

consider the cosmic microwave radiation as the only background radiation.

In Fig. 9, we present the variation of  $c\text{-MgC}_2$  excitation ( $T_{\text{ex}}$ ) and brightness ( $T_{\text{B}}$ ) temperatures as a function of gas density. For densities below  $10^5 \text{ cm}^{-3}$ ,  $T_{\text{B}}$  increases linearly with  $n_{\text{H}_2}$ . At low density, the  $T_{\text{B}}$  magnitude is lower for transitions involving high energy levels because these levels are weakly populated under the typical physical conditions of IRC+10216 CSE. At high densities, the reverse is seen since highly excited rotational states start to be efficiently populated by collisions. We however note that for densities below  $10^5 \text{ cm}^{-3}$ , the population of  $c\text{-MgC}_2$  levels is highly sensitive to the gas density and therefore  $c\text{-MgC}_2$  represents a good gas density tracer in CSE.

Fig. 9 shows however that  $T_{\text{ex}}$  remains below 4 K for densities up to a few  $10^5 \text{ cm}^{-3}$ , and the lines become fully thermalized for  $n_{\text{H}_2} \geq 10^6 - 10^7 \text{ cm}^{-3}$ . At low density, the  $T_{\text{ex}}$  values of all lines are quite similar and close to the background radiation. From this finding, a main conclusion for the astrophysical modelling of  $c\text{-MgC}_2$  observation in IRC+10126 CSE can be drawn: LTE conditions are not met, as the required density ( $n_{\text{H}_2} \geq 10^6 - 10^7 \text{ cm}^{-3}$ ) is too high for the IRC+10216 envelope located 30 arcsec from the centre of the star. Such behaviour can be explained by the high magnitude of the  $c\text{-MgC}_2$  dipole moment, more than by the magnitude of rate coefficients that are not particularly low. At the opposite, we can see that the excitation temperatures of the observed lines are similar and

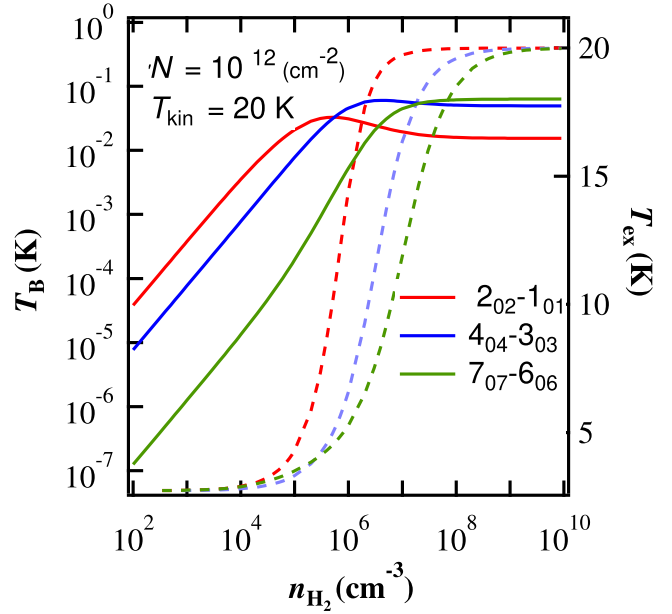


**Figure 9.** Excitation (dashed lines) and brightness (solid lines) temperatures, for selected  $c\text{-MgC}_2$  transitions, as a function of the  $\text{H}_2$  density. The calculations are performed for a column density ( $N = 10^{12} \text{ cm}^{-2}$ ). The kinetic temperatures considered correspond to 20 K.

**Table 2.** Comparison of excitation temperatures (in K) calculated in this work using non-LTE radiative transfer modelling with those reported by Changala et al. (2022), who employed a rotational diagram analysis. Gas densities are expressed in  $\text{cm}^{-3}$ .

line	$T_{\text{k}} = 20 \text{ K}$		$T_{\text{k}} = 30 \text{ K}$		$T_{\text{k}}^{\dagger} = 22 \pm 13 \text{ K}$
	$n_{\text{H}_2} = 5 \times 10^3$	$n_{\text{H}_2} = 2 \times 10^4$	$n_{\text{H}_2} = 5 \times 10^3$	$n_{\text{H}_2} = 2 \times 10^4$	
$2_{02} \rightarrow 1_{01}$	2.816	3.065	2.835	3.133	$6 \pm 1$
$4_{04} \rightarrow 3_{03}$	2.767	2.870	2.778	2.909	$6 \pm 1$
$4_{23} \rightarrow 3_{22}$	2.760	2.848	2.768	2.879	$6 \pm 1$
$4_{22} \rightarrow 3_{21}$	2.765	2.866	2.775	2.904	$6 \pm 1$
$5_{05} \rightarrow 4_{04}$	2.767	2.867	2.782	2.918	$6 \pm 1$
$5_{42} \rightarrow 4_{41}$	2.747	2.797	2.750	2.812	$6 \pm 1$
$5_{41} \rightarrow 4_{40}$	2.747	2.797	2.750	2.812	$6 \pm 1$
$5_{23} \rightarrow 4_{22}$	2.766	2.868	2.780	2.917	$6 \pm 1$
$6_{06} \rightarrow 5_{05}$	2.778	2.900	2.806	2.987	$6 \pm 1$
$7_{07} \rightarrow 6_{06}$	2.814	3.002	2.883	3.184	$6 \pm 1$
$7_{25} \rightarrow 6_{24}$	2.826	3.045	2.899	3.240	$6 \pm 1$

Note. The superscript  $\dagger$  refers to Changala et al. (2022)

that it may be possible to consider a single excitation temperature for all the lines.

To assess the validity of the excitation temperature adopted by Changala et al. (2022), we compare this value with the  $T_{\text{ex}}$  derived from our escape probability calculations, as shown in Table 2. To represent realistic physical conditions in IRC+10216, we use gas densities of  $5 \times 10^3$  and  $2 \times 10^4 \text{ cm}^{-3}$ , corresponding to radius of 40 and 15 arcsec, respectively (Guélin et al. 2018). The excitation temperatures from our escape probability calculations are all around  $T_{\text{ex}} \approx 3 \text{ K}$  and show a very moderate increase, up to 10 per cent, with increasing gas density. Such value is in contradiction with the rotational diagram analysis of Changala et al. (2022) who found a value of  $6 \pm 1 \text{ K}$ , which overestimates our result by a factor of two. As shown in Fig. 9, these excitation temperatures can be obtained for high gas

**Table 3.** Comparison of rotational temperatures (in K) calculated in this work using population ratio with those reported by Changala et al. (2022) from a rotational diagram analysis. Gas densities are expressed in cm<sup>-3</sup>.

Initial: final levels used for the $T_{\text{rot}}$ calculation	$T_k = 20$ K		$T_k = 30$ K	
	$n_{\text{H}_2}$ $5 \times 10^3$	$n_{\text{H}_2}$ $2 \times 10^4$	$n_{\text{H}_2}$ $5 \times 10^3$	$n_{\text{H}_2}$ $2 \times 10^4$
2 <sub>21</sub> : 1 <sub>01</sub>	19.14	19.50	31.03	32.08
4 <sub>41</sub> : 2 <sub>21</sub>	16.48	16.61	23.20	23.51
4 <sub>41</sub> : 1 <sub>01</sub>	17.06	17.23	24.72	25.15
5 <sub>41</sub> : 4 <sub>04</sub>	37.34	33.76	144.88	96.28
5 <sub>41</sub> : 4 <sub>22</sub>	24.08	23.17	42.70	39.23
5 <sub>23</sub> : 4 <sub>04</sub>	8.08	8.12	9.35	9.46
5 <sub>41</sub> : 5 <sub>23</sub>	37.19	45.12	20.59	23.61
5 <sub>41</sub> : 5 <sub>05</sub>	40.15	50.80	21.03	24.42

densities, specifically  $n_{\text{H}_2} > 10^5$  cm<sup>-3</sup> for the 2<sub>02</sub> → 1<sub>01</sub> transition and  $n_{\text{H}_2} > 10^6$  cm<sup>-3</sup> for the other transitions. In our models, only the cosmic microwave radiation (2.7 K) has been considered. However, IRC+10216 CSE is subject to strong radiative radiation (González-Alfonso et al. 1998) so that the energy levels of *c*-MgC<sub>2</sub> can be also populated by radiative pumping as observed for other molecules. The introduction of radiative pumping, may play a significant role in the excitation processes of *c*-MgC<sub>2</sub> and may allow to get a higher excitation temperature for the observed lines. A more sophisticated non-LTE modelling, that takes into account the radiative pumping, is then required to accurately interpret the observational spectra of *c*-MgC<sub>2</sub>. Alternatively, another explanation for the deviation between the predicted and observed rotational temperature could be that the present *c*-MgC<sub>2</sub>-H<sub>2</sub> rate coefficients, estimated from *c*-MgC<sub>2</sub>-He ones are significantly underestimated. Then, despite such a large underestimate would be surprising, we have multiplied the *c*-MgC<sub>2</sub>-He rate coefficients by a factor of 10 and performed new excitation calculations. We found that the excitation temperatures are slightly increasing (up to 4–5 K) but always remain below the observed value of 6 K. Radiative pumping is hence the most probable mechanism for the excitation of *c*-MgC<sub>2</sub> in the circumstellar gas.

Finally, as stated in the introduction, Changala et al. (2022) used a two-temperatures model for the rotational diagram analysis since it was not possible to use the same rotational temperature for the levels within a *k*-ladder and for levels belonging to different *k*-ladders. In their study, Changala et al. (2022) considered that the population of energy levels of different *k*-ladders is that of a thermalized media [e.g. the rotational temperature ( $T_{\text{rot}}$ ) equals the kinetic temperature ( $T_k$ )]. For the levels belonging to two different *k*-ladders, we have analysed their populations obtained from the radiative transfer calculations and we have determined a  $T_{\text{rot}}$  based on these populations. Initially, we performed the analysis for only the lowest energy levels of each *k*-ladder ( $j_{k_a, k_c} = 1_{01}, 2_{21}, \text{ and } 4_{41}$ ). The results are shown in Table 3.

As one can see, the rotational temperatures derived from our radiative transfer calculations are in reasonable agreement with the kinetic temperature and seems to confirm the hypothesis of Changala et al. (2022). However, when we have determine a  $T_{\text{rot}}$  from the population of higher rotational levels [especially those with  $j = 5$  and 4 that were also used by Changala et al. (2022)], we found that the derived  $T_{\text{rot}}$  deviate significantly from the kinetic temperature in some case. In their study, Changala et al. (2022) found a kinetic temperature of  $T_k = 22 \pm 13$  K, a value that contains a significant uncertainties that is actually confirmed by our models. It means that the population of the energy levels between the different *k*-ladders is not systematically thermalized and can significantly deviate from

the LTE value (despite the ‘average  $T_{\text{rot}}$ ’ obtained by probing the populations of many rotational states may be not so different from the kinetic temperature). Such behaviour can probably be related to the magnitude of the rate coefficients involving levels in different *k*-ladders that are much weaker than those for transitions between levels within the same *k*-ladder and not high enough in magnitude to maintain LTE conditions.

## 5 CONCLUSION

The first 3D PES for the *c*-MgC<sub>2</sub>-He collisional system has been computed using the CCSD(T)-F12/aug-cc-pVTZ level of theory. Using the analytical representation of this interaction potential and the close-coupling quantum mechanical approach, we have determined state-to-state excitation cross sections for *c*-MgC<sub>2</sub> induced by collisions with He, for total energies up to 300 cm<sup>-1</sup>. By thermally averaging these cross sections, we obtained rate coefficients for transitions involving rotational energy levels with an internal energy below 44 cm<sup>-1</sup>, for temperatures up to 30 K.

We also performed radiative transfer calculations with the new rate coefficients using the escape probability formalism and considering the cosmic microwave radiation as the only background radiation. For typical gas densities and kinetic temperatures in the outer envelope of IRC+10216 (where *c*-MgC<sub>2</sub> has been detected), we found an excitation temperature of 3 K for all the detected lines, showing the collision are inefficient for exciting *c*-MgC<sub>2</sub> under such physical conditions. Such behaviour can probably be explained by the magnitude of the *c*-MgC<sub>2</sub> dipole moment.

The excitation temperature obtained by our models differs by a factor of two from the excitation temperature reported by Changala et al. (2022) using a rotational diagram analysis. This seems to indicate that the excitation of *c*-MgC<sub>2</sub> in the IRC+10216 CSE is weakly due to neutral colliders and could possibly be driven by radiative pumping. We also found that the population of the energy levels between different *k*-ladders differ significantly from LTE conditions, contrary to what was assumed by Changala et al. (2022). Hence, it seems that *c*-MgC<sub>2</sub> is not a good thermometer for IRC+10216 CSE.

## ACKNOWLEDGEMENTS

The authors acknowledge the European Research Council (ERC) for funding the COLLEXISM project No. 811363, the Programme National ‘Physique et Chimie du Milieu Interstellaire’ (PCMI) of Centre National de la Recherche Scientifique(CNRS)/Institut National des Sciences de l’Univers (INSU) with Institut de Chimie (INC)/Institut de Physique (INP) co-funded by Commissariat à l’Energie Atomique (CEA) and Centre National d’Etudes Spatiales (CNES). FL acknowledges the Institut Universitaire de France. We Acknowledge Jose Cernicharo and Fehmi Khadri for helpful discussions.

## DATA AVAILABILITY

The MgC<sub>2</sub>-He rate coefficients will be available on the BASECOL data base (Dubernet et al. 2024).

## REFERENCES

- Agúndez M., Fonfría J. P., Cernicharo J., Kahane C., Daniel F., Guélin M., 2012, *A&A*, 543, A48  
Alexander M. H., Manolopoulos D. E., 1987, *J. Chem. Phys.*, 86, 2044



- Arthurs A. M., Dalgarno A., 1960, *Proc. R. Soc. London, Ser. A*, 256, 540
- Bouhafs N., Lique F., Faure A., Bacmann A., Li J., Guo H., 2017, *J. Chem. Phys.*, 146, 064309
- Boys S. F., Bernardi F., 1970, *Mol. Phys.*, 19, 553
- Cabezas C. et al., 2023, *A&A*, 672, L12
- Cernicharo J., Guélin M., Pardo J., 2004, *ApJ*, 615, L145
- Cernicharo J. et al., 2019, *A&A*, 630, L2
- Changala P. et al., 2022, *ApJ*, 940, L42
- Dubernet M. et al., 2024, *A&A*, 683, A40
- Endres C. P., Schlemmer S., Schilke P., Stutzki J., Müller H. S., 2016, *J. Mol. Spectrosc.*, 327, 95
- Faure A., Crimier N., Ceccarelli C., Valiron P., Wiesenfeld L., Dubernet M., 2007, *A&A*, 472, 1029
- Feller D., 1992, *J. Chem. Phys.*, 96, 6104
- González-Alfonso E., Cernicharo J., van Dishoeck E. F., Wright C. M., Heras A., 1998, *ApJ*, 502, L169
- Guélin M. et al., 2018, *A&A*, 610, A4
- Hampel C., Peterson K. A., Werner H.-J., 1992, *Chem. Phys. Lett.*, 190, 1
- Hutson J., Green S., 1994, Molscat Computer Code, Version 14 (MAR 95), Distributed by Collaborative Computational Project No. 6 of the Science and Engineering Research Council, UK
- Itono S., Takano K., Hirano T., Nagashima U., 2000, *ApJ*, 538, L163
- Kendall R. A., Dunning T. H., Jr, Harrison R. J., 1992, *J. Chem. Phys.*, 96, 6796
- Knizia G., Adler T. B., Werner H.-J., 2009, *J. Chem. Phys.*, 130, 054104
- Lique F., Toboła R., Klos J., Feautrier N., Spielfiedel A., Vincent L., Chałasiński G., Alexander M., 2008, *A&A*, 478, 567
- Mauron N., Huggins P., 2010, *A&A*, 513, A31
- Pardo J. et al., 2022, *A&A*, 658, A39
- Petrie S., 1996, *MNRAS*, 282, 807
- Tsuji T., 1973, *A&A*, 23, 411
- Tuo J. et al., 2024, *ApJS*, 271, 45
- Turner B., 1991, *ApJ*, 376, 573
- Urzúa-Leiva R., Denis-Alpizar O., 2020, *ACS Earth Space Chem.*, 4, 2384
- Van der Tak F., Black J. H., Schöier F., Jansen D., van Dishoeck E. F., 2007, *A&A*, 468, 627
- Werner H. et al., 2015, A Package of Ab Initio Programs. University of Cardiff Chemistry Consultants (UC3), Cardiff, Wales, UK. Available at: <http://www.molpro.net>
- Wernli M., Wiesenfeld L., Faure A., Valiron P., 2007, *A&A*, 464, 1147

This paper has been typeset from a  $\text{\TeX}/\text{\LaTeX}$  file prepared by the author.